Measurement 152 (2020) 107317

Contents lists available at ScienceDirect

Measurement

journal homepage: www.elsevier.com/locate/measurement

Novel laser triangulation measurement method for screw rotor profile under multi-factor constraints

Bin Yao, Zhiqin Cai *, Jie Lu, Xiaofan Ma, Binqiang Chen

School of Aerospace Engineering, Xiamen University, Xiamen 361005, China

ARTICLE INFO

Article history:
Received 30 August 2019
Received in revised form 20 November 2019
Accepted 22 November 2019
Available online 27 November 2019

Keywords:
Screw rotor profile
Laser triangulation
Multi-factor constraints
Laser beam positioning
Laser-measurement trajectory planning
Error compensation

ABSTRACT

In order to achieve optimal control of the screw rotor process, a novel measurement method using laser triangulation under multi-factor constraints was introduced to achieve online measurement of the screw rotor profile. This method involved the integration of a 4-axis motion system, which is used to adjust the laser probe, with a laser displacement sensor (LDS), which is used to measure the screw rotor profile. Firstly, the effect of laser beam positioning on measurement accuracy was analyzed experimentally in conjunction with an improved LDS error compensation model. Then, according to the characteristics of rotor profiles, a laser-measurement trajectory planning algorithm for the rotor profile under multi-factor constraints was developed. Finally, the comparison study between the traditional contact measurement (P65) and the proposed measurement demonstrates that the proposed method has not only kept the advantages of traditional contact measurement, but also shown good performances and high measuring precision.

1. Introduction

To provide desired performance of the twin screw compressor, proper manufacturing and accurate assembly of the screw rotor, the core component of the compressor is vital. Recently, a variety of screw machinery products have become increasingly popular in many areas, such as traditional mechanical manufacturing, petrochemicals, refrigeration, aerospace, and national defense. Consequently the requirements for technical indicators, such as working efficiency and service life of screw machinery products, have become increasingly higher. With the advent of the 3D helical surface in screw rotor design, the surface characteristics and the curvature of helical surface have changed a lot. The common screw rotor profile is composed of cycloid, point, arc, involute and other plane curves [1], measurement has become much more complex, requiring high accuracy for the measurement of the screw rotor profile to ensure the required accuracy, reliability, and conformity. The form grinding method is widely used in the processing of screw rotor, which has high manufacturing accuracy, but affected by some factors before and during grinding [2]. Indexing error, profile error, helix error and coaxality are the main errors, which are caused by the uneven indexing, the wear of grinding wheel and installation error in grinding. Among them, the tooth profile error has more influence on the manufacturing accuracy. In this paper, the profile error of screw rotor is studied.

In the field of coordinate measuring machine measurement, accurate and efficient measurement of unknown rotor profiles has been the focus. Klingelnberg GmbH, Hexagon Metrology, Zeiss, Holroyd and Hexagon Metrology GmbH et al. established high-precision methods for screw rotor detection. For the 3D helical surface for screw rotor, its normal vectors vary with different measured points, while conventional 2D measuring methods have the inevitable radius compensation. Based on double-measurement method and 3D radius compensation, a novel measurement method for unknown rotor profile of screw compressor was proposed by Ji [3]. The selection basis and compensation technology of one-dimensional probe sphere radius for screw rotor were studied by Teng [4]. Aiming at difficulties in obtaining parameter lead by measuring spiral line with coordinate measuring machine equipped with touch trigger probe, a new method was proposed to keep procedure of lead measurement from spiral scan by Zhao [5]. The main difficulties of the contact measurement are as follows: 1) due to the twist of helical surface, the measuring rod is easy to interfere with the measured surface. Therefore, if automatic measurement trajectory planning is adopted, critical information will be lost or incomplete, which puts forward higher requirements for measurement trajectory planning. 2) Because of the probe radius, it is difficult to measure the characteristic boundary of helix surface accurately. Moreover, at the boundary of the screw rotor,

* Corresponding author.
E-mail address: caizhiqin@xmu.edu.cn (Z. Cai).

https://doi.org/10.1016/j.measurement.2019.107317
0263-2241/

the measurement data may be inaccurate due to the possible run-out and sliding of the probe. Therefore, an efficient and accurate compensation algorithm determines the final measurement accuracy, and thus should be resolved. 3) Contact probe, especially three-dimensional scanning probe, is expensive and vulnerable to measurement environment. 4) the detecting needle of contact methods breaks easily and may scratch the screw surface.

The screw rotor belongs to a kind of helical surface product. Non-contact methods for measuring the screw surface have been proposed in recent years, which can eliminate the contact induced errors of contact measurement and improve the measurement accuracy. An automatic non-contact measuring system for extracting the parameters of a screw thread was developed by Tong [6]. A non-contact vibration sensor based on fiber bragg grating (FBG) sensing, and applied to measure vibration of turbine rotor dynamic balance platform was presented by Li [7]. An automatic non-contact measuring system integrated using a light curtain, a high-accuracy linear encoder and a motion platform, for the thread profile of a ball screw was developed by Zhao [8]. A kind of intellectualized test method of small pitch of thread parameters, it can realize non-contact, rapid and accurate measurement of the thread pitch screw parameters was put forward by Chao [9]. By designing a customized measuring head with a perfect threaded geometry, a novel measuring method for virtual pitch diameter of a thread was proposed by Qiu [10]. By leveraging a NC tool rest to drive the LDS so as to acquire the data of the thread axial section contours, an on-machine precision measurement method for a certain API thread was proposed by Dong [11]. Based on the geometric analysis of the axial section projection image of screw thread, the calculation formula of thread profile distortion was deduced, and the corresponding compensation algorithm was given by Chen [12].However, there are few studies on the non-contact measurement method for helical surface of screw rotor.

Laser triangulation, a non-contact measurement method with significant development prospects, has been widely used to measure the three-dimensional contours of various complex surfaces [13]. Owing to the measurement accuracy of laser displacement sensors (LDS) and mechanical positioning systems, which can reach micron-level precision, the laser triangulation method can be applied to achieve the required accuracy, reliability, and conformity in a more efficient and convenient manner, compared with other non-contact measurement methods. To improve the measurement accuracy and reliability of the LDS, the influences of the inclination angle, the scanning distance, object color and reflectivity were presented by Vukašinović [14]. By analyzing the error caused by different colors of a measurand surface, a compensation method to improve the accuracy of laser triangulation measurements was proposed by Li [15]. By obtaining the pixel-grey curves of the image, standardization and iterative interpolation, a new algorithm to deal with the data collected in laser triangulation measurement was proposed by Wu [16].To improve the measurement accuracy of LDS, the effects of the scan depth, surface roughness, inclination angle and azimuth angle were investigated experimentally, and a practical measurement strategy considering the spatial posture of the LDS were presented by Li and Sun [17]. Aiming to improve the precision of optical distance measurement sensors based on laser triangulation, a calibration model that involves the parameters of the camera, lens and laser positions to find the best accuracy was proposed by Idrobo-Pizo [18]. To suppress laser dithering, a scheme to reduce the effect of laser beam directional dithering, which was composed of a collimated red laser, a laser beam pointing control setup, a receiver lens, and a charge-coupled device, was proposed by Yang [19]. By using particle swarm optimization (PSO), a possible approach to determine the light source positions highly accurate was presented by Christian [20], which effectively reduces the overall measurement error of the system. To summarize, the measurement accuracy of LDS is affected by many factors, including the surface characteristics of the measured object (e.g., roughness, color, material), spatial posture of the LDS, ambient temperature, and light intensity. To further increase the measurement accuracy, the influence of spatial posture parameters for the LDS, such as rotation angle and deflection angle, which are rarely considered, is analyzed, and the error compensation model is improved.

In this paper, by leveraging a 4-axis motion system to drive the LDS so as to acquire the data of the screw rotor profile, a novel non-contact based on laser triangulation, high accuracy and automatic area measurement method for the screw rotor profile under multi-factor constraints was developed. In this method, 1) according to the principle of laser triangulation and considering the influence of the spatial posture of the LDS, the system error occurred were fully analyzed and compensated. The improved 4-D error compensation model not only considers the influence of inclination angle and scanning distance, but also the deflection angle and rotation angle, which are often ignored. 2) In order to obtain the minimum measurement error, aiming at the problem that the complex rotor profile through mechanical and optical path interference causes undesirable blind zones in detection, a laser-measurement trajectory planning algorithm, ensure that the detection is conducted along or near the normal direction of each measured point on the rotor profile without any interference, for the rotor profile was proposed.

To do these, Section 2 introduces the measuring principle and instrument configuration. A detailed description of the measuring algorithm is provided in Section 3. Section 4 describes an error analysis of the proposed system. Section 5 proposes a plan for laser measurement of the screw rotor profile under multi-factor constraints. Section 6 presents the measurement results and verification for the screw rotor, and Section 7 provides the conclusions.

2. Measuring principle and instrument configuration

The instrument configuration of the laser measuring system for the screw rotor profile, as shown in Fig. 1, is composed of a mechanical unit and measurement unit. The mechanical unit, a 4-axis motion system, composed of an X-axis, Y-axis, Z-axis, and rotational C-axis. The measured workpiece is fixed on the Fig. 9 C-axis. The axes of motion are positioned by signal feedback through a Reynesau grating. Meanwhile, the LDS is fixed at the end of X-axis and moves along the other three axes. To realize the non-contact measurement of screw rotor, the normal direction of the measured point is rotated to the horizontal direction by

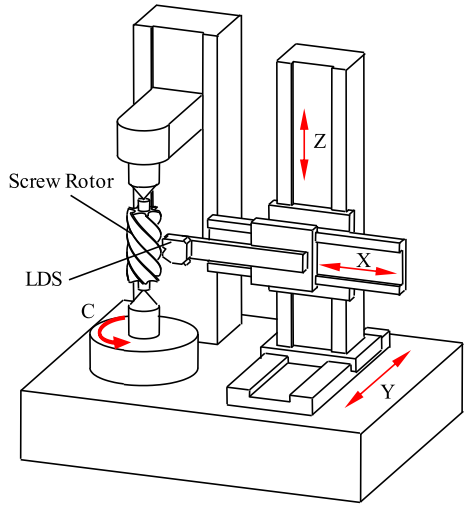

Fig. 1. 4-axis motion system based on LDS.

controlling the C-axis of the precision turntable, whereas motion along the Y-axis is controlled to make the laser beam hit the position of the desired point precisely to realize detection in the direction of the normal vector. Finally, to ensure a reasonable scanning distance between the measured point and the laser probe, motion of the probe is controlled along the X-axis.

For this, it is necessary to convert the measured value of the LDS from coordinate system S_s to the machine reference frame S_M. It needs to establish the following coordinate systems, as shown in Fig. 2.

(1) The coordinate system S_s (o_s-$x_s y_s z_s$) of the LDS. The zero position of the LDS is defined as the original point. The directions of the 3 axes are consistent with the $X/Y/Z$-axis, respectively.
(2) Machine reference frame S_M (o_M-$x_M y_M z_M$). When the measuring machine is in the zero state and the scan depth of the LDS is 0 mm, this position is defined as the origin point. The directions of the 3 axes are consistent with the $X/Y/Z$-axis of the machine tool respectively.
(3) The motion coordinate system S_1 (o_1-$x_1 y_1 z_1$) of the rotor helical surface. The direction of the z_1 is consistent with the C-axis, and the plane $\triangle o_1 x_1 y_1$ is parallel to the plane $\triangle$OXY.

As shown in Fig. 2, the coordinate formula $\boldsymbol{r}_M = [x_M, y_M, z_M, 1]^T$ in machine reference frame S_M can be obtained through the coordinate transformation matrix M_{MS} from S_s to S_M.

$$\boldsymbol{r}_M = M_{MS} \cdot \boldsymbol{r}_S = M_{M1} \cdot \boldsymbol{r}_1 + \Delta \boldsymbol{E} \tag{1}$$

where $\boldsymbol{r}_S = [x_S, y_S, z_S, 1]^T$ is the measured value of the LDS in the coordinate system S_s. $\boldsymbol{r}_1 = [x_1, y_1, z_1, 1]^T$ is the theoretical data points of measured rotor in the coordinate system S_1, which can be obtained by the results in Section 3.1. The unit vector of the laser-beam in S_s coordinate system are l, m, n, and the corresponding length is d (readout directly from the LDS), then $\boldsymbol{r}_S = [ld, md, nd, 1]^T$. M_{M1} represents the coordinate transformation matrix from S_1 to S_M. $\Delta \boldsymbol{E}$ represent the measuring error of the system, which can be obtained from Section 4, Then

$$\begin{aligned} \boldsymbol{r}_M &= \begin{bmatrix} 1 & 0 & 0 & x_{M0} \\ 0 & 1 & 0 & y_{M0} \\ 0 & 0 & 1 & z_{M0} \\ 0 & 0 & 0 & 1 \end{bmatrix} \cdot \begin{bmatrix} ld \\ md \\ nd \\ 1 \end{bmatrix} = \begin{bmatrix} x_{M0} + ld \\ y_{M0} + md \\ z_{M0} + nd \\ 1 \end{bmatrix} \quad \text{or} \\ \boldsymbol{r}_M &= \begin{bmatrix} \cos\varphi_c & -\sin\varphi_c & 0 & \Delta x \\ \sin\varphi_c & \cos\varphi_c & 0 & \Delta y \\ 0 & 0 & 1 & \Delta z \\ 0 & 0 & 0 & 1 \end{bmatrix} \cdot \begin{bmatrix} x_1 \\ y_1 \\ z_1 \\ 1 \end{bmatrix} + \Delta \boldsymbol{E} \end{aligned} \tag{2}$$

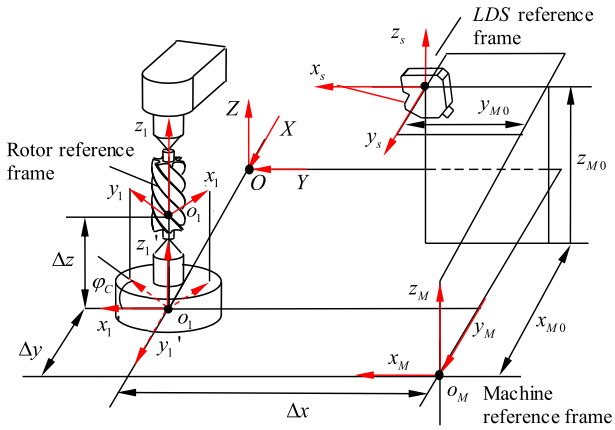

Fig. 2. Coordinate transformation process.

where (x_{M0}, y_{M0}, z_{M0}) represents the grating value.

3. Measuring algorithm

The rotor profile curve is obtained through piecewise cubic spline interpolation. The detailed processing methods and steps are described as follows.

3.1. Rotor profile curve data fitting

The motion coordinate system $S_1(o_1$-$x_1 y_1 z_1)$ for the helical surface of the male rotor and the fixed coordinate system $S(o$-$xyz)$ for the rotor profile are shown in Fig. 3. The line of intersection between the helical surface and the plane perpendicular to the axis of the screw rotor is defined as the rotor profile. Because of the unknown rotor profile of the screw compressor, the profile is usually given in the form of discrete data. To obtain the normal vectors of the helical surface and rotor profile, fitting this discrete data with a function is necessary. In this study, a cubic spline fitting function with the cumulative chord length as a parameter is used.

Assuming that the discrete data of rotor profile is (x_i, y_i), $i = 1,2\ldots n$, s_i is cumulative chord lengths

$$\begin{cases} s_0 = 0 \\ s_i = \sum_{j=0}^{i} \sqrt{(x_j - x_{j-1})^2 + (y_j - y_{j-1})^2}, i = 1, 2, \ldots, n \end{cases} \tag{3}$$

A cubic spline function is constructed, and the coordinate formula $\boldsymbol{r}$ of the rotor profile is as follows:

$$\boldsymbol{r}(s_i) = [x(s_i), y(s_i)] \tag{4}$$

and

$$\begin{cases} x(s_i) = a_0 + a_1 s_i + a_2 s_i^2 + a_3 s_i^3 \\ y(s_i) = b_0 + b_1 s_i + b_2 s_i^2 + b_3 s_i^3 \end{cases} \tag{5}$$

where, a_0, a_1, a_2, a_3 and b_0, b_1, b_2, b_3 are coefficients of cubic spline functions $x = x(s_i)$ and $y = y(s_i)$, respectively.

For the coordinate system S_1, the screw surface equation $\boldsymbol{r}_1$ based on the discrete data points $\boldsymbol{r}$ of the male rotor can be determined, as follows:

$$\begin{aligned} \boldsymbol{r}_1(s_i, \theta) &= [x_1, y_1, z_1] \\ &= [x(s_i)\cos(\theta) \mp y(s_i)\sin(\theta), y(s_i)\cos(\theta) \pm x(s_i)\sin(\theta), p\theta] \end{aligned} \tag{6}$$

where, p and θ are the helix parameters, "+"means right-handed and "−" means left-handed.

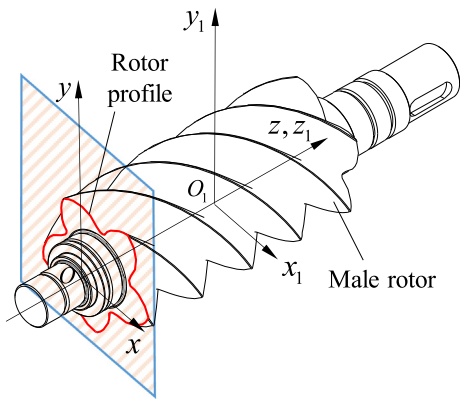

Fig. 3. Geometric structure of screw rotor.

3.2. Spatial posture of helical surface

Based on the 4-axis motion system, the spatial posture of the LDS in the retrieval of the screw rotor profile is illustrated in Fig. 4. *P* is the measured point of the rotor profile, **EP** shows the path of the incident light of the laser probe, the scanning distance is h (which is located at the measuring range of LDS, as shown in Table.1), **PF** is the path of the receiving light, and $\triangle EPF$ is a laser measuring plane. The normal directions of the rotor profile and helica surface are $\boldsymbol{n}$ and $\boldsymbol{N}$, respectively. The coordinate system $S_p(P\text{-}x_py_pz_p)$ is established. The z_p-axis is parallel to the axis of the screw rotor. The x_p-axis coincides with $\boldsymbol{n}$. The laser measurement plane $\triangle EPF$ is parallel to the z_p-axis.

The normal direction $\boldsymbol{n}$ of rotor profile can be expressed as

$$\boldsymbol{n}(s_i) = \left(-\frac{\partial y}{\partial s_i}, \frac{\partial x}{\partial s_i}\right) \tag{7}$$

The helical surface equation can be expressed by Eq. (6), and the normal direction $\boldsymbol{N}$ of helical surface can be expressed as

$$\begin{cases} \boldsymbol{N}(s_i,\theta) = \frac{\boldsymbol{n}_1(s_i,\theta_i)}{\sqrt{\boldsymbol{n}_1(s_i,\theta)\cdot\boldsymbol{n}_1(s_i,\theta)}} \\ \quad\quad = \left[p\frac{\partial y_1}{\partial s}, -p\frac{\partial x_1}{\partial s}, \pm x_1\frac{\partial x_1}{\partial s} \pm y_1\frac{\partial y_1}{\partial s}\right] \\ \boldsymbol{n}_1(s_i,\theta) = \frac{\partial \boldsymbol{r}_1(s_i,\theta)}{\partial s_i} \times \frac{\partial \boldsymbol{r}_1(s_i,\theta)}{\partial \theta} \end{cases} \tag{8}$$

1) The angle between vectors $\boldsymbol{n}$ and $\boldsymbol{N}$ is defined as the incident angle α

$$\alpha = \arccos\left(\frac{\boldsymbol{N}(s_i,\theta)\cdot\boldsymbol{n}(s_i)}{|\boldsymbol{N}(s_i,\theta)||\boldsymbol{n}(s_i)|}\right) \tag{9}$$

2) The angle between vector $\boldsymbol{n}$ and plane $\triangle EPF$ is defined as the deflection angle γ

$$\gamma = \arccos\left(\frac{\boldsymbol{EP}\cdot\boldsymbol{n}(s_i)}{|\boldsymbol{EP}||\boldsymbol{n}(s_i)|}\right) \tag{10}$$

3) The angle between vector **EP** and plane $\triangle EPF$ is defined as the rotation angle β.

Therefore, the spatial posture of the LDS is defined by scanning distance *h*, the incident angle α, the rotation angle β, and the deflection angle γ.

4. Error analysis for the proposed system

The performance of this measurement system depends on the transmission accuracy of mechanical unit and measuring error of laser unit. Under the precondition of ensuring the transmission accuracy of the proposed system, this study mainly addresses the measurement error of the laser unit, which is primarily a function of the scanning distance *h*, incident angle α, rotation angle β, and deflection angle γ. Thus, these factors should be analyzed and calibrated to minimize the measuring error.

Table 1
Main parameters of LK-H050 laser displacement sensor.

Parameters	LK-H050
Installation mode	Diffuse reflection
Measuring Center Distance	50 mm
Measuring range	±10 mm
Spot diameter	50um
Linear	±0.02% F.S.
Reproducibility	0.025um
Temperature characteristic	0.01% F.S./°C
Resolution	2um

4.1. Error source analysis

The LDS is a precision optical instrument designed based on the principle of laser triangulation. Its defocusing phenomenon will cause the dispersion of image points, thereby reducing the measurement accuracy [9].

As shown in Fig. 5, the principle errors of laser measurement system under the influence of scanning distance *h*, incident angle α, rotation angle β, and deflection angle γ are analyzed. *P* is the measured point on the inclined plane, and the inclined angle is α. *R* is the effective radius of the receiving lens, L_0 is the distance between the measured point *P* and center M_1 of the receiving lens, θ is the angle between vectors **KA** and $\mathbf{AM_1}$, ω_0 is the angle between vector $\mathbf{PM_1}$ and normal vector **n** of measured point *P*, and *d* is the distance from the center M_1 of the receiving lens to the starting point *K* of the laser beam. The spatial coordinate system $S(O\text{-}XYZ)$ and the follow-up coordinate system $S'(O'-X'Y'Z')$ are established with point *P* as the origin. The Z-axis coincides with the laser beam, the X-axis is on the inclined plane, and the Y- axis is perpendicular to the inclined plane. When the LDS rotates around the Z-axis (i.e., the measuring plane *MPK* rotates around the *PK*-axis to the measuring plane M_1PK), the center point *M* to the point M_1, the corresponding angle is defined as rotation angle β.

As shown in Fig. 5, the normal vector of the measured point-*P* is $\boldsymbol{PN} = (\sin\alpha, 0, cos\alpha)$, and $\boldsymbol{PM}_1 = (d\cos\beta, d\sin\beta, L_0\cos(\theta+\delta))$. Because parameter $\delta$is very small, vector $\mathbf{PM_1}$ can be expressed as

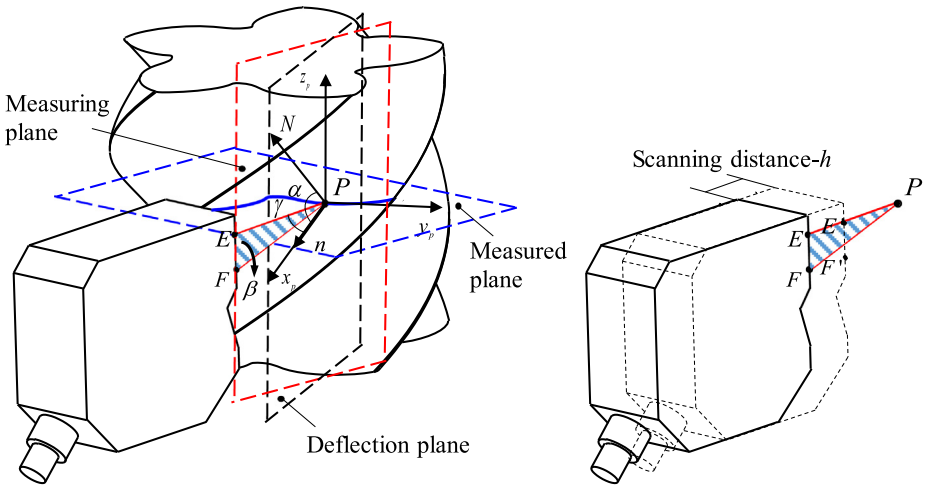

Fig. 4. The spatial posture of the LDS.

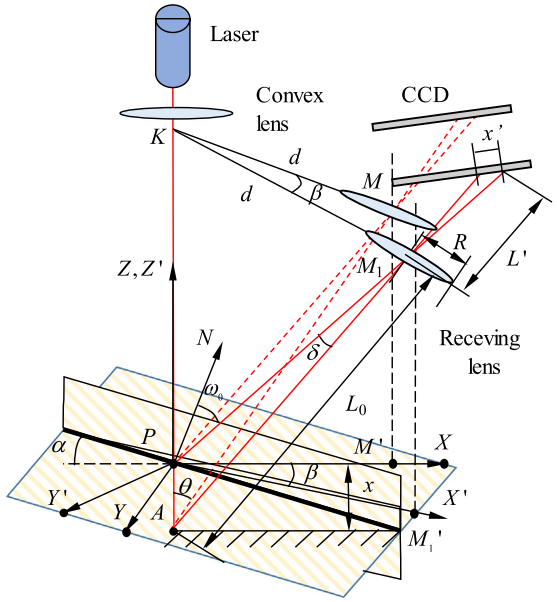

Fig. 5. Measurement of LDS on inclined surface.

$$\boldsymbol{PM}_1 = (d\cos\beta, d\sin\beta, L_0\cos\theta) \tag{11}$$

According to the angle formula between vectors **PN** and $\mathbf{PM_1}$, it can be seen that

$$\cos\omega_0 = \frac{\boldsymbol{PM}_1 \cdot \boldsymbol{PN}}{|\boldsymbol{PM}_1||\boldsymbol{PN}|} \approx \frac{d\sin\alpha\cos\beta + L_0\cos\alpha\cos\theta}{L_0} \tag{12}$$

Because $d \approx L_0\sin\theta$, and

$$\tan\omega_0 = \sqrt{\frac{1}{(\sin\alpha\cos\beta\sin\theta + \cos\alpha\cos\theta)^2} - 1} \tag{13}$$

Laser measurement errors under the influence of three factors-scanning distance h, incident angle α, and rotation angle β can be expressed as follows.

$$\begin{aligned} E_{a1} &= |\boldsymbol{M}_1\boldsymbol{K}|_{\alpha\neq0,\beta\neq0} - |\boldsymbol{MK}|_{\alpha=0,\beta=0} \\ &= \frac{R^2L'x\cos\theta}{L_0^3}\left(1 + \frac{2x\cos\theta}{L_0}\right)\left(\sqrt{\frac{1}{(\sin\alpha\cos\beta\sin\theta+\cos\alpha\cos\theta)^2} - 1} - \tan\theta\right) \end{aligned} \tag{14}$$

It can be seen from Eq. (14) that the change in the laser measurement error increases with the increase in incident angle α and rotation angle β. The larger the incident angle α or the rotation angle β is, the greater effect it has on the measurement error induced by the rotation angle β or the incident angle α. In addition, when the incident angle α varies in a small range, the small effect of the incident angle on the measurement error.

4.2. Calibration method of laser beam posture

Eq. (14) reflects a sensor imaging model based on geometrical optics. However, under actual conditions, when a laser beam is incident on the measured surface, the scattered field is distributed in all directions of space. The spatial distribution of scattered light field is extremely complex, which makes it difficult to solve the mathematical model in engineering application. To study the error model of laser triangulation under actual conditions, the effects of the scanning distance, inclination angle, rotation angle, and deflection angle are investigated experimentally, and a practical prediction model based on RBF(Radical Basis Function) neural network is presented.

A certain surface inclination angle can be built, as shown in Fig. 6. Based on the coordinate systems shown in Fig. 5, the machine reference frame S (o-xyz), and motion coordinate system S'' (o''-$x''y''z''$) are established based on the rotational axis (C-axis), respectively. The z-axis and z''-axis coincide with the C-axis. P represents the measured point of the surface, **PN** represents the normal direction of measured surface, **EP** represents the laser-beam, **PF** represents the receiving laser-beam, and $\triangle EPF$ represents the measuring plane of *LDS*. The plane $\triangle LMH$ can be built through laser-beam **EP** and the normal direction **PN**, and **EP** is parallel to **LM**. The vertical line oz of **LM** is established through measured point P, and o is the intersection. Reclosing and vertical to **LM** respectively, the coordinate system S (o-xyz) can be established.

(1) **Inclination angle.** The angle between the laser-beam **EP** and the normal direction **PN** is defined as inclination angle α. On the plane Δxoz, when the normal direction **PN** and the receiving laser-beam **PF** are defined at the different (same) side to laser-beam **EP**, the inclination angle is positive (negative), as shown in Fig. 6.
(2) **Rotation angle.** On the plane Δxoy, the angle between the plane $\Delta xoz$and the plane $\Delta x''o''z''$ is defined as the rotation angle β, which can be obtained by controlling the rotation angle of the turntable. The rotation angle is positive (negative) when the measured surface is revolving in the anti-clockwise (clockwise) direction.
(3) **Deflection angle.** The angle between the measurement plane $\triangle EPF$ and the plane Δxoz is defined as deflection angle γ; it is positive (negative) when it is close to (away from) the positive direction of the y-axis.

The deflection angle γ can be obtained by converting it into the inclination angle α' and the rotation angle β'. To accomplish this conversion, the measuring plane $\triangle E'PF'$ can be obtained by the plane $\triangle EPF$ rotates the deflection angle γ around the x-axis, and the converted plane $\triangle E'PF'$, $\triangle L'M'H'$ and the coordinate system S' (o'-$x'y'z'$) can be obtained. Then, the inclination angle α' can be confirmed by the normal direction **PN** of the measured surface and laser-beam **E′P**.

Considering the effect of the deflection angle γ, the inclination angle α' can be expressed as

$$\alpha' = \arccos\left(\frac{\boldsymbol{PN} \times \boldsymbol{E'P}}{|\boldsymbol{PN}| \times |\boldsymbol{E'P}|}\right) = \arccos\left(\frac{\cos\gamma}{\sqrt{1+\tan\alpha^2}}\right) \tag{15}$$

For *LDS*, the normal vector of the plane $\triangle PHX'$ can be represented as

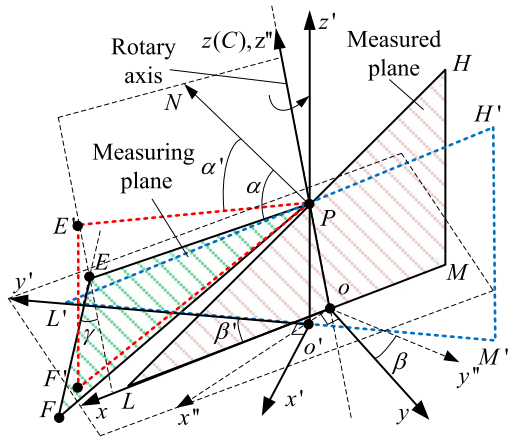

Fig. 6. Relationship between swing angle with incident angle and rotation angle.

$$\boldsymbol{n}' = \begin{bmatrix} 0 \\ \frac{\cot\alpha'}{\sin\gamma}\cos\theta_z + \sin\theta_z \\ -\frac{\cot\alpha'}{\sin\gamma}\sin\theta_z + \cos\theta_z \end{bmatrix} \tag{16}$$

where θ_z represents the angle between the laser-beam **EP** and the z'-axis.

Then, the relationship between the deflection angle γ with inclination angle α' and rotation angle β' can be expressed as

$$\begin{aligned} \beta' &= \arccos\left(\frac{\boldsymbol{n}'\times\boldsymbol{OY}}{|\boldsymbol{n}'|\times|\boldsymbol{OY}|}\right) \\ &= \arccos\left(\frac{\frac{\cot\alpha'}{\sin\gamma}\cos\theta_z+\sin\theta_z}{\sqrt{\left(\frac{\cot\alpha'}{\sin\gamma}\cos\theta_z+\sin\theta_z\right)^2+\left(-\frac{\cot\alpha'}{\sin\gamma}\sin\theta_z+\cos\theta_z\right)^2}}\right) \end{aligned} \tag{17}$$

4.3. Laser beam calibration experiment

Based on the above conclusions, the measurement error calibration of the LK-H050 laser displacement sensor is conducted as a function of inclination angle, rotation angle, and scanning distance. The specific parameters of the LDS are shown in Table 1, where the installation range of the LDS is 40 mm to 50 mm, the scanning distance of the LDS is −10 mm to 10 mm and the resolution of LDS is 2um. The error correction is obtained through the following experimental devices: an NC machining center, LDS (LK-H050 produced by Keyence), laser interferometer (XL-80 produced by Renishaw), sine gauge, standard gauge block, and indexing plate, as shown in Fig. 7. By composing the sine gauge and gauge blocks with different heights, simultaneously controlling the C-axis of the NC machining center, the spatial posture of the LDS can be simulated, as shown in Fig. 7. Before the experiment, the spatial posture of the LDS should be precisely adjusted to ensure that the laser beam is parallel to the Z-axis, and the optical path of the interferometer does not shift when moving along the *Z*-axis. Moreover, the LDS should move along the *Z*-axis within the effective measurement range.

The error model of the deflection angle can be converted to those of inclination angle and rotation angle based on Eq. (17). Therefore, only three spatial posture parameters-inclination angle, rotation angle, and scanning distance are calibrated and analyzed.

Through the error calibration experiments, 2310 sets of measurement data for the LDS and interferometers are obtained. By comparing the LDS data with that from the interferometers, the corresponding measurement errors of each spatial posture can be obtained.

Fig. 8(a) shows the influence of scanning distance h(h = −10 m m ~ 10 mm) on the measurement accuracy of the LDS at different inclination angles α (10°, 20°, 30°, and 40°) and rotation angles β (0°, 40°, 80°, 90°, 100°, 140°, 180°). Fig. 8(b) shows the influence of inclination angle α on the measurement accuracy of the LDS under different scanning distances h (−8, −4, 0, 4, 8 mm), in the case of rotation angle β = 0°. Fig. 8(c) shows the influence of rotation angle β on the measurement accuracy of the LDS at different inclination angles α (5°, 10°, 20°, 30°, 40°, and 45°), in the case of scanning distance h = 5 mm.

Based on the above error data, a four-dimensional error compensation model of the LDS in full measuement range is established based on RBF neural network, in which X-, Y-, and Z-axes represent the inclination angle α, rotation angle β, and scanning distance h, respectively, and the color represents the error value as shown in Fig. 9.

The conclusions are as follows:

As shown in Fig. 8(a), 1) the change in the measurement error increases with increase in scanning distance h, with constant inclination angle α and rotation angle β. 2) On the fixed inclination angle α and scanning distance h, the measurement error is changeable with rotation angle β. Moreover, when the rotation **angle** β is equal to 0 or 180 (°), the error is the largest. The error is small within an inclination angle α range of 80 to 90(°). 3) On the fixed rotation angle β and scanning distance h, the change of the measurement error increases with the increase of inclination angle α.

As shown in Fig. 8(b), 1) with respect to fixed scanning distance h, the change in the measurement error increases with the increase in inclination angle α. The error varies approximately linearly within an inclination angle α range of −30° to + 30°. In other areas, the measurement error varies nonlinearly. The slope change of the error curve increases with increase in inclination angle α, and the effect of inclination angle α on the measurement error increases. 2) When the scanning distance h is equal to 0 mm, the measurement error remains constant with the change in inclination angle α, and the measurement error is 0 mm.

As shown in Fig. 8(c), 1) with respect to fixed inclination angle α, the measurement error varies regularly with the change in rotation angle β. 2) When both inclination angle α and rotation angle β are at maximum, the positive value of the measurement error is at maximum. When the inclination angle α is at maximum and the rotation angle β is at minimum, the negative value of the measurement error is at minimum. 3) When rotation angle approaches 0° or 180°, the variation rate of the measurement error increases with increase in inclination angle α.

To summarize, to reduce the impact of spatial posture on the LDS, it is recommended to 1) maintain a lower scanning distance h such that the linearity of the measurement error can be improved and the compensated measurement accuracy can be ensured. 2) Adjust the rotation angle β, and keep it stable at 90°, which lessens

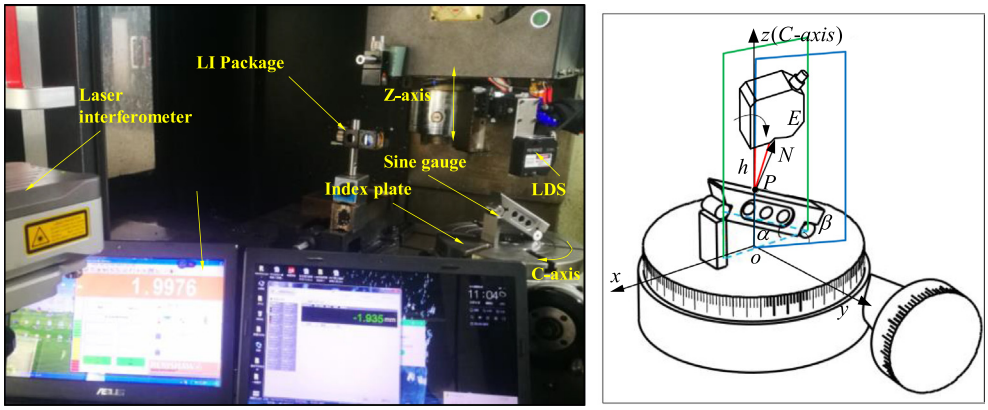

Fig. 7. Error calibration experiment of the LDS.

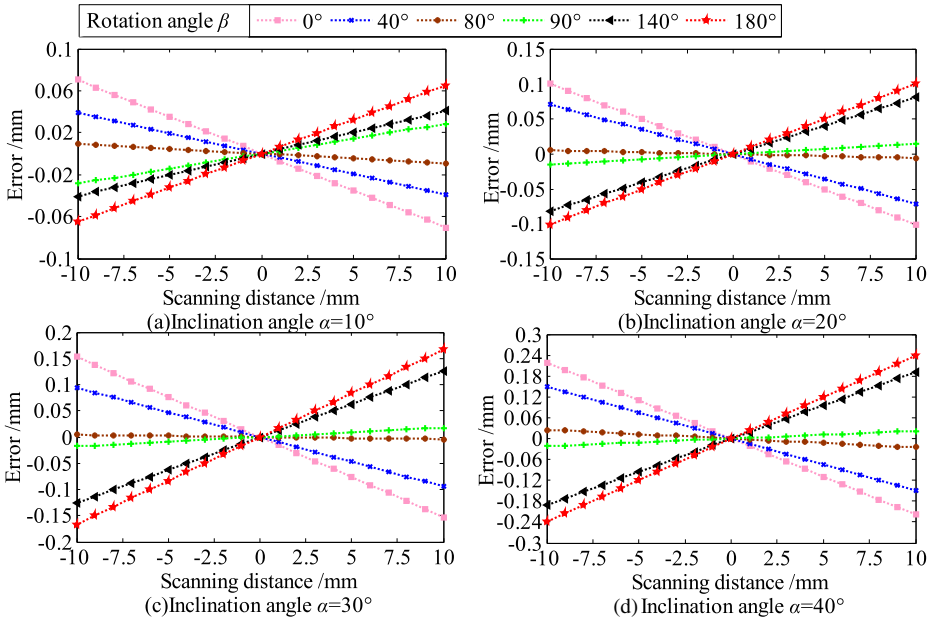

(a) The influence of scanning distance h on measurement error

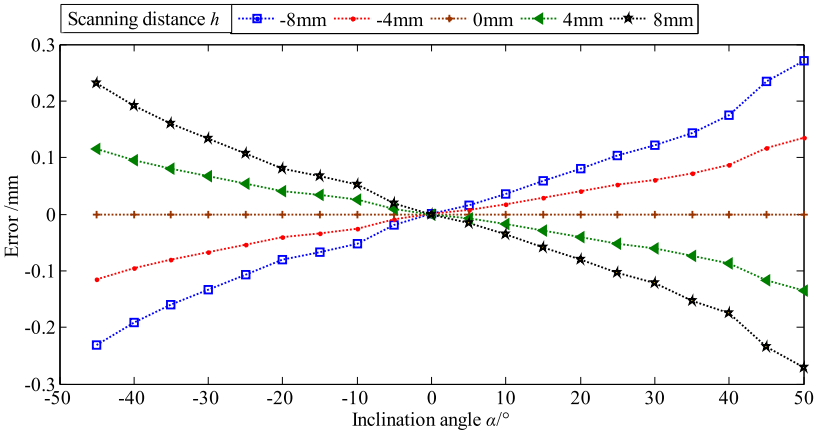

(b) The influence of inclination angel α on measurement error

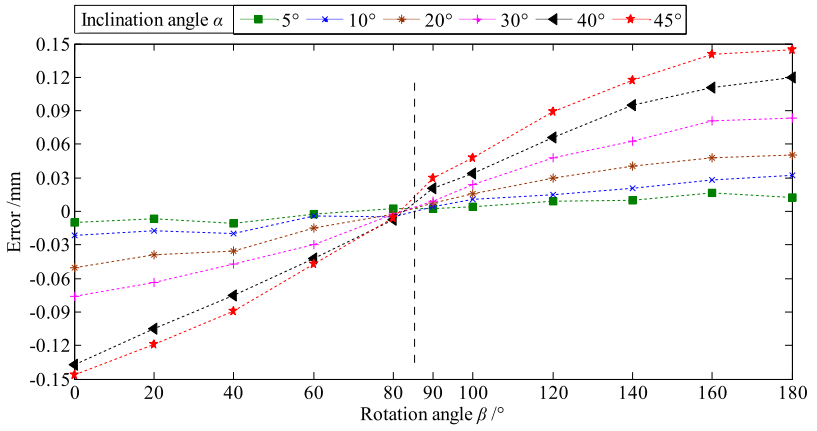

(c) The influence of rotation angel β on measurement error

Fig. 8. The influence of the LDS posture on measurement error.

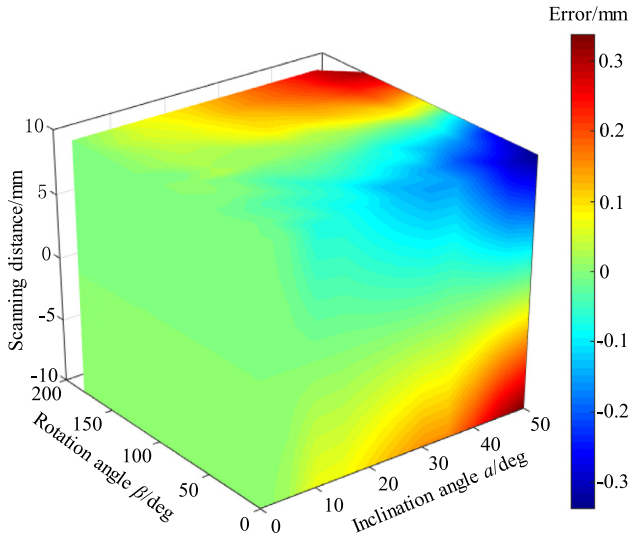

Fig. 9. Four-dimensional error compensation model of the LDS.

the impact of β on the measurement error. 3) Give attention to the effects of β and the converted deflection angle λ, although the effect of these two angles on measurement accuracy is less compared with that of inclination angle α.

5. Laser-measurement trajectory plan for the end-profile of a screw rotor

The complex rotor profile through mechanical and optical path interference causes undesirable blind zones in detection, as shown in Fig. 10. Based on the analysis results of Section 4, a multi-factor-constrained laser-detection trajectory plan for the end-profile of a screw rotor is proposed. This plan considers the effects of optical path interference, mechanical interference, scanning distance, and spatial posture. By adjusting the relative posture between the LDS and the screw rotor, the plan for the path of the laser beam, approaching the normal direction of the measured point automatically without interference, is realized.

5.1. Laser detection trajectory plan for non-blind-zone detection

To ensure that the laser beam coincides with the normal vector direction of the sampled point in detecting the non-blind zone, the data points can be extracted by coordinating the rotation angle of the screw rotor (around the C-axis), the movement along the X/Y-axis, and the measurement displacement h of the LDS. As shown in Fig. 11, d is the measuring distance, and point P_m is the measurement starting point. The specific measurement steps are as follows:

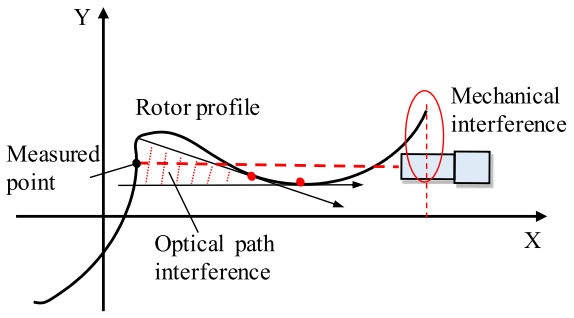

Fig. 10. Mechanical interference and optical path interference.

1) Calculate the normal vector and rotation angle of starting point P_m on the rotor profile. Rotate the normal vector until parallel to the X-axis, That is, the normal vector coincides with the laser beam.
2) Adjust the spatial posture of the LDS until the laser beam is parallel to the X-axis. Then, coordinate the movement of the LDS along the X- and Y-axes to the theoretical point of point P_m, where the laser beam is maintained at a stable measuring distance d, and record the current LDS reading d_0.
3) Calculate the angle θ_m between two adjacent points P_{m+1} and P_m on the rotor profile. Control the screw rotor rotating about the C-axis by adjusting θ_m to ensure that the normal vector of point P_{m+1} is parallel to the X-axis, and the current coordinate value of point P_{m+1} is determined. Then, the relative coordinate $(\Delta x_m, \Delta y_m)$ between points P_{m+1} and P_m can be obtained.
4) Coordinate the LDS to move Δx_m and Δy_m along the X- and Y-axes, respectively. Then, confirm that the laser beam coincides with the normal vector of point P_{m+1} and record the current LDS reading $d_0 + \Delta d_{m+1}$.
5) Repeat steps 2) and 3) to complete the measurement trajectory in the non-blind zone.

5.2. Laser detection trajectory plan for blind-zone detection

To obtain the maximum degree of approximation to the normal direction of the measured points, in the case that the optical path does not interfere with the measured helical surface and the sensor does not collide with the measured workpiece, a measurement trajectory plan for detection in the blind zone is presented. As shown in Fig. 12, P_n is the current measured point (#1 in Fig. 12), and the current LDS reading is $d_0 + \Delta d_n$. The angle between the normal directions of the next measured point P_{n+1} and the current measured point P_n is θ_n.

As can be seen from #4 in Fig. 12, the normal vector extension line of point P_{n+1} interferes with the rotor profile. That is, if the normal direction of this point coincides with the optical path, optical path interference will eventually occur. Therefore, the laser beam cannot coincide with its normal direction for data point acquisition. To ensure that the laser beam approximates the normal direction of point P_{n+1} to the maximum extent, specific measurement steps are performed as follows:

(1) The measuring value of point P_{n+1} can be determined by the laser beam coincident with the tangent vector of the measured point (#6 in Fig. 12). The actual rotation angle θ_n' between two adjacent points P_{n+1} and P_n can be expressed as

$$\theta_n' = \theta_n - \gamma_n \tag{18}$$

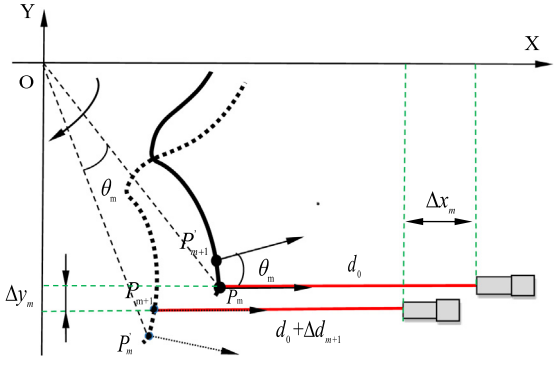

Fig. 11. Measurement trajectory planning in non-blind zone.

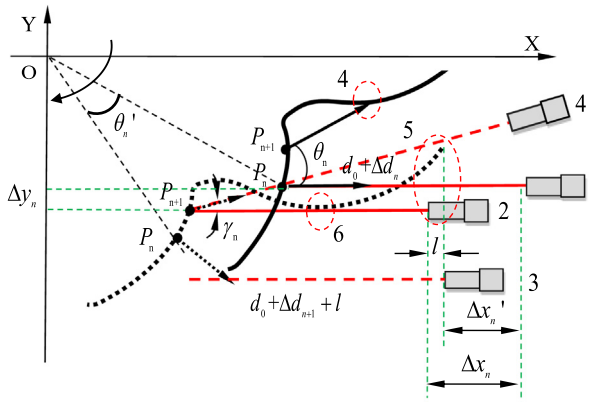

Fig. 12. Measurement trajectory planning in blind zone.

where γ_n represents the deflection angle of measured point P_{n+1}.

(2) Control the screw rotor rotating about the C-axis with θ_n' to ensure the tangent vector of point P_{m+1} is parallel to the X-axis, and the current coordinate value of point P_{n+1} is solved; then, the relative coordinate $(\Delta x_n, \Delta y_n)$ between adjacent points P_{n+1} and P_n can be obtained.
(3) Coordinate the LDS to move Δx_n and Δy_n along X- and Y-axes, respectively. Then, confirm that the laser beam coincides with the tangent vector of point-P_{n+1}(#2 in Fig. 12), and record the current LDS reading $d_0 + \Delta d_{n+1}$.
(4) If there is mechanical interference between the LDS and the rotor profile (#5 in Fig. 12), the X-axis should be controlled to remove the slot (#3 in Fig. 12). The current reading of the LDS is $d_0 + \Delta d_{n+1} + l$, and the corresponding motion values of X-, Y-, and C-axes are $(\Delta x_n', \Delta y_n, \theta_n')$, in which

$$\Delta x_n' = \Delta x_n - l \tag{19}$$

(5) Repeat the steps 1)–4) to complete the measurement trajectory in blind zone.

5.3. The detection process of rotor profile

To summarize, the detection process of the rotor profile based on laser triangulation method is shown in Fig. 13(a), and the detail procedure of measuring algorithm is shown in Fig. 13(b).

It should be noted that to realize the measurement path plan of the rotor profile under multi-factor constraints, the conclusions of Section 4.3 apply.

1) The measurement plane of the LDS is as vertical as possible to the end-section of the screw rotor, i.e., the rotation angle is 0° or 180° to increase the non-blind zone.
2) When measuring the rotor profile points, the LDS should be maintained at an optimum measuring distance d by controlling the motion along the X-axis (i.e., scanning distance h = 0). When the measured point is in the mechanical interference zone, the scanning distance should be adjusted to be small as possible to reduce its influence on the measurement accuracy.
3) The normal vector direction of the measured point should be as far as possible for detection, so that the deflection angle is 0°. When the normal vector direction of the measured point is located at the blind zone, the deflection angle is adjusted to be as small as possible.

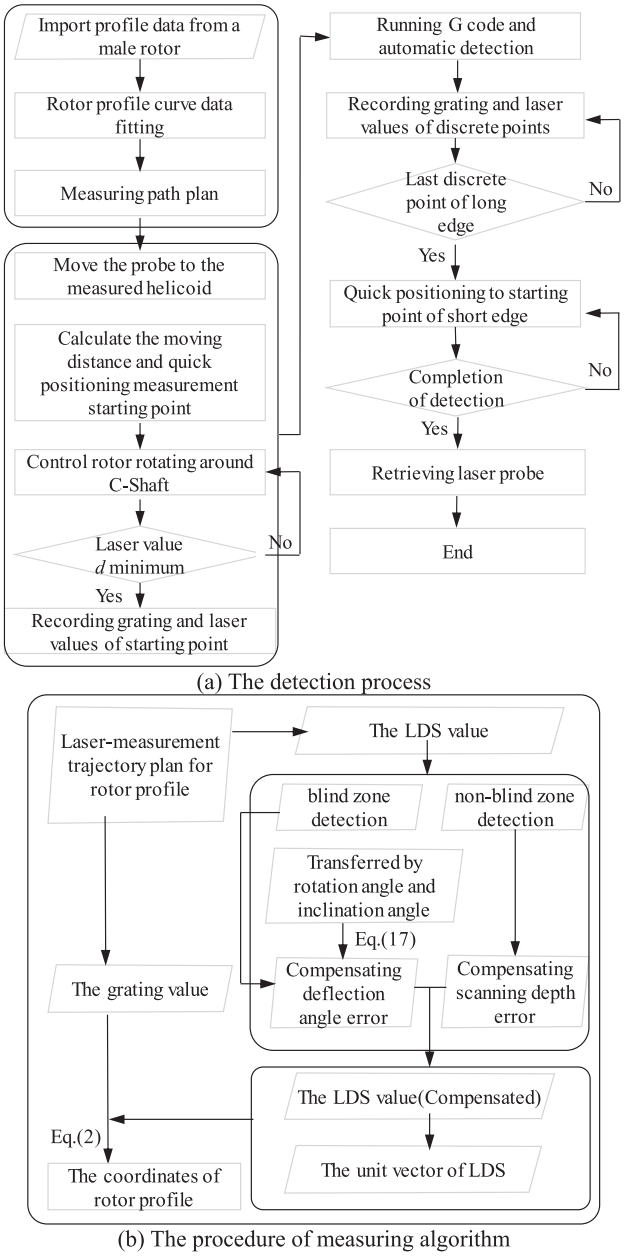

Fig. 13. The detection of rotor profile.

4) When the measured surface of rotor is polished and inclined, which is a common situation in screw rotor profile measurement, the surface roughness and the measured point will different from the theoretical condition. For the laser triangulation measurement, the compensation affected by the inclination angle and surface roughness will be affected. To reduce the impact of this situation, the laser beam calibration experiment need to be carried out under the same roughness conditions, and maintain a lower scanning distance to weaken the effect of spatial posture parameters for the LDS.

6. Measurement and verification results for the screw rotor

6.1. Experimental setup

The structural parameters for a typical screw rotor are shown in Table 2. The measurement trajectory plan of the rotor profile is

Table 2
Structural parameters of the screw rotor.

Thread direction	Teeth number	External diameter /mm	Root diameter / mm	Lead/ mm	Helical angle/°
Right	5	116	71	240	42.011

given in Fig. 14, in which Zone-2 is the measurement blind zone, Zones-1, −3, and −4 are the measurement non-blind zones, and the measurement sequence is from Zone-1 to Zone-4.

As shown in Fig. 14, the C-axis is the rotating axis of the screw rotor, X-axis is parallel to the laser beam, and Y-axis is vertical to the laser beam. The specific measurement process is as follows:

1) The first point of the short edge is defined as the initial point of measurement, which is shown in Fig. 14, and the coordinate value in coordinate system S_1 is (46.909, −34.091). The LDS is controlled to move 57.982 mm negatively along the X-axis and 0.991 mm positively along the Y-axis (as shown in Fig. 15(b)). Meanwhile, the screw rotor is rotated counterclockwise around the C-axis of 34.802° (as shown in Fig. 15 (a)) to ensure the normal vector direction of the starting point is parallel to the X-axis.
2) The non-blind Zone-1 on the short edge is measured. The C-axis rotates clockwise, and the LDS positively moves along both X- and Y-axes, as shown in Fig. 15(b).
3) The blind Zone-2 on the short edge is measured. The C-axis rotates counterclockwise, and the LDS moves negatively along both X- and Y-axes.
4) The non-blind Zone-3 on the transition curve is measured. The C-axis rotates counterclockwise, the LDS negatively moves along the Y-axis, and moves negatively then positively along the X-axis.
5) The non-blind Zone-4 on the long curve is measured. The C-axis rotates clockwise, the LDS positively moves along the Y-axis, and moves negatively along the X-axis.

During the entire measuring process, the Z-axis remains unchanged, and the overall variation of the C-axis is the final rotation of the single rotor profile measurement. The projection of the measured trajectory on the XY plane is shown in Fig. 14.

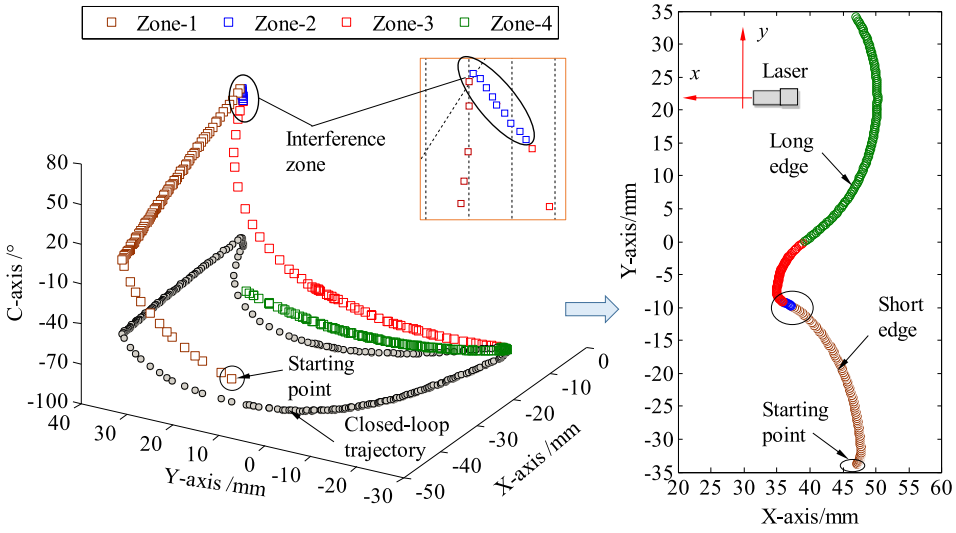

Fig. 14. Trajectory planning for laser measurement of male rotor.

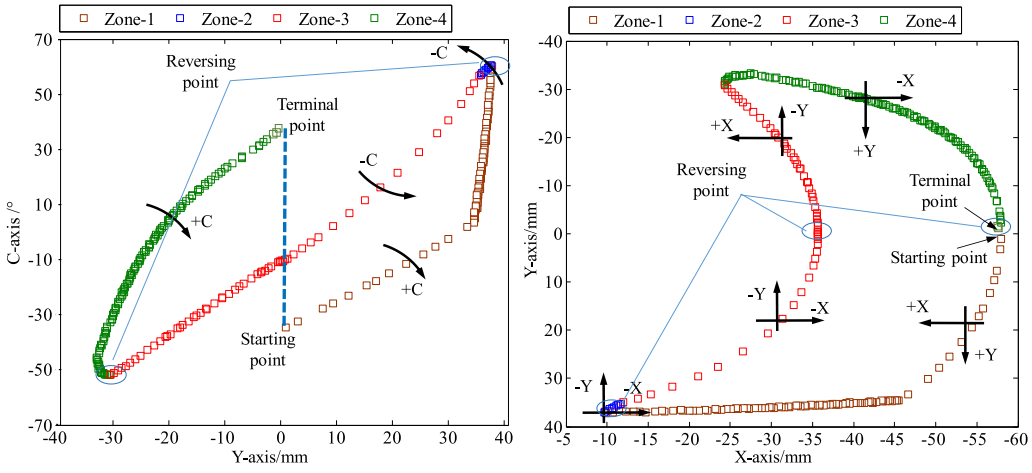

Fig. 15. Variation planning along X,Y and C axes.

Fig. 16. Experimental platform of LDS for measuring screw rotor.

Because the last point of the long edge is close to the first point of the short edge of the next rotor profile, the entire trajectory forms a closed loop, i.e., the overall variation of the X-axis and Y-axis is almost unchanged, thus verifying the correctness of the trajectory plan.

6.2. Measurement experiment and error compensation analysis of screw rotor

1) Measurement experiment by LDS

According to the analysis results of the measurement trajectory planning, there is no mechanical interference in the measurement of the rotor profile. Therefore, the LDS can be stabilized at the scanning distance h = 0 for measurement. However, to verify the accuracy of the error compensation model, the LDS is stabilized at a scanning distance h of about 0.5 mm. Meanwhile, the proposed method is compared with the P65 measurement results to further verify the accuracy of the model. The proposed measuring instrument configuration is shown in Fig. 16.

To compensate for the measuring error of the rotor profile, the normal vectors **n** and **N** of the measured point and the angle between the two are calculated by Eq. (17). According to the measurement path plan, the spatial posture of the measured points can be obtained. The deflection angle can be converted into inclination angle α and deflection angle β, as shown in Fig. 17. As shown in Fig. 17(a), in the blind zone, both the rotation angle and deflection angle of the LDS are equal to 0°. That is, the laser beam coincides with the normal direction of the measured points.

In the measurement blind zone, the deflection angle γ can be converted into inclination angle α and rotation angle β, and the transformed spatial posture is shown in Fig. 17 (b). The transformed deflection angle is equal to 0°, whereas the rotation angle and the inclination angle change to some extent. The measurement error prediction models under the influence of the inclination angle α and the rotation angle β can be used to obtain the measurement error caused by deflection angle γ. The measurement errors before and after compensation in the measurement blind area are shown in Table 3. As shown in Table.3, due to the measurement error, the laser probe only can be stabilized at a scanning distance h of about 0.5 mm i.e. each measuring position has a certain scanning distance error, which is defined as the conversed value (CV). The error after compensation can be obtained by searching inclination angle and rotation angle in 4D error compensation model. The Accuracy after compensation can be obtained by the superposition of conversed value (CV) and error, and the measurement accuracy of micron level can be achieved.

2) Measurement experiment by P65

To verify the measurement accuracy of the proposed method, the comparative experiment use screw rotor professional measurement software of the German Klingelnberg P65 automatic CNC controlled measuring center to measure the coordinates of the rotor profile (Fig. 18(a)). The main work flow is shown in Fig. 18 (b). During the experiments, in order to avoid the probe intervenes with the measurement rotor surface, the appropriate probe must be selected, i.e. the intersection angle of the probe and the intersecting line (formed by the tangent plane and the pitch plane at

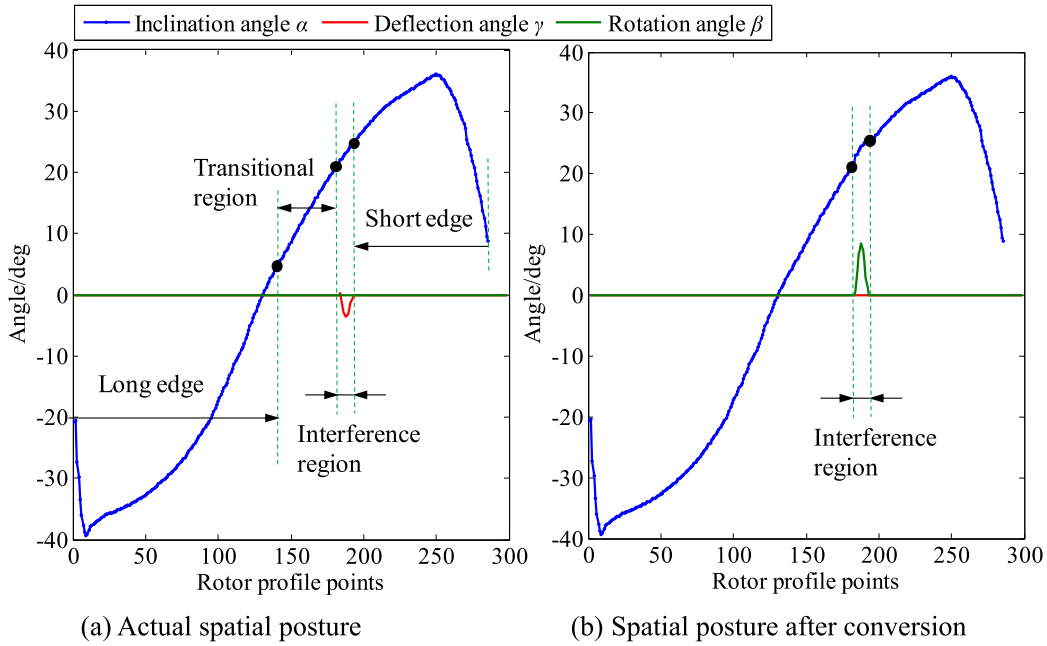

Fig. 17. Spatial posture of screw rotor.

Table 3
Measurement results of blind zone.

Data point	Measurements		Spatial posture			Error compensation model				Accuracy after compensation
	Laser value	CV	IA	DA	RA	IA	DA	RA	Error	
184	0.507	0.007	21.94	0.249	0	22.94	0	0.62	−0.005	0.002
185	0.501	0.001	22.18	−1.76	0	23.25	0	4.31	−0.005	−0.004
186	0.499	−0.001	22.60	−2.86	0	23.77	0	6.84	−0.006	−0.007
187	0.498	−0.002	22.89	−3.17	0	24.10	0	7.46	−0.006	−0.008
188	0.497	−0.003	23.20	−3.65	0	24.47	0	8.45	−0.006	−0.009
189	0.516	0.016	23.54	−3.23	0	24.75	0	7.37	−0.006	0.010
190	0.517	0.017	23.87	−2.45	0	24.99	0	5.52	−0.006	0.011
191	0.515	0.015	24.19	−1.31	0	25.22	0	2.92	−0.007	0.008
192	0.514	0.014	24.42	−0.57	0	25.42	0	1.26	−0.007	0.007

lA, Inclination angle; RA, Rotation angle; DA, Deflection angle.

measured point) must be greater than zero, moreover, be as small as possible [21].

6.3. Results analysis

Errors in the screw rotor profile cause noise and vibration of the rotor pair when the screw compressor is not running smoothly, which increases the energy consumption of the screw compressor. The contact line leakage of the screw compressor is increased and the energy efficiency ratio of the compressor is reduced by making the clearance between the female and male rotors uneven or the contact line discontinuous. Because the screw profile is usually expressed in the form of discrete points, the profile error is mainly used as the overall evaluation criterion of the present screw rotor profile. The rotor profiles before and after compensation are shown in Fig. 19, and the errors of each measured point before and after compensation are shown in Fig. 20.

To verify the correctness of the theory, the comparison results between the compensated profile and P65 are shown in Fig. 19. From the figure, it can be seen that the changes in the profile morphology measured by the two methods are basically the same. The profile errors fluctuate significantly in the long and short edges of the rotor profile, but smaller in the transition curve and the blind zone. For further analysis, the measurement errors of the two methods are shown in Fig. 20.

We assume that the average error $\bar{\delta}$ and standard deviation$\sigma$of the proposed method are as follows:

$$\begin{cases} \bar{\delta} = \dfrac{\sum_{i=1}^{n} \delta_i}{n} \\ \sigma = \sqrt{\dfrac{\sum_{i=1}^{n} \left(\delta_i - \bar{\delta}\right)^2}{n-1}} \end{cases} \tag{20}$$

(1) In the range of 3σ, any profile point error F_α may occur in the interval $(\bar{\delta}-3\sigma,\bar{\delta}+3\sigma)$. That is, the measuring error of the proposed method is E = −3.4 μm–15.9 μm and the average error is 5.9um, while the measuring error of P65 is E = −4.5 μm–16.9 μm and the average error is 5.8 um. The results of error comparison show that the measurement compensated accuracy is in good agreement with that of P65. The results of the two methods show that the manufacturing error of the rotor is mainly positive, which provides a favorable reference for the profile modification of shaped grinding wheel. Generally, the accuracy requirement of rotor profile measurement is −15 μm–15 μm. Therefore, the above analysis results show that the rotor is qualified. However, the manufacturing accuracy of rotor can be further improved, by using the measurement results to guide the profile modification of the formed grinding wheel.
(2) The comparison results before and after compensation show that the proposed error compensation method has a significant compensation effect. The long and short edges of the rotor profiles exhibit relatively large compensation values.

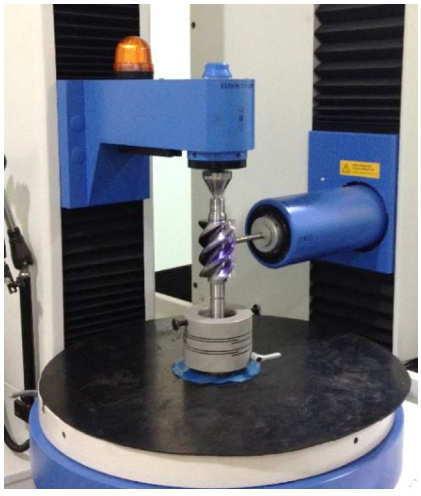

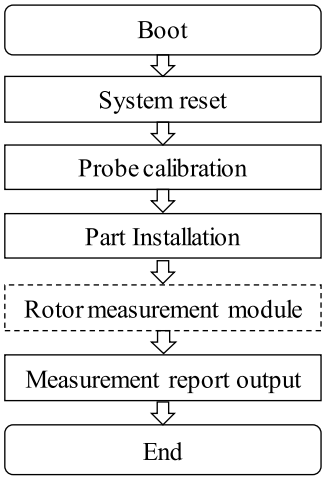

(a) Instrument configuration of P65 (b) Work flow of measuring rotor profile

Fig. 18. Experimental platform of P65 for measuring screw rotor.

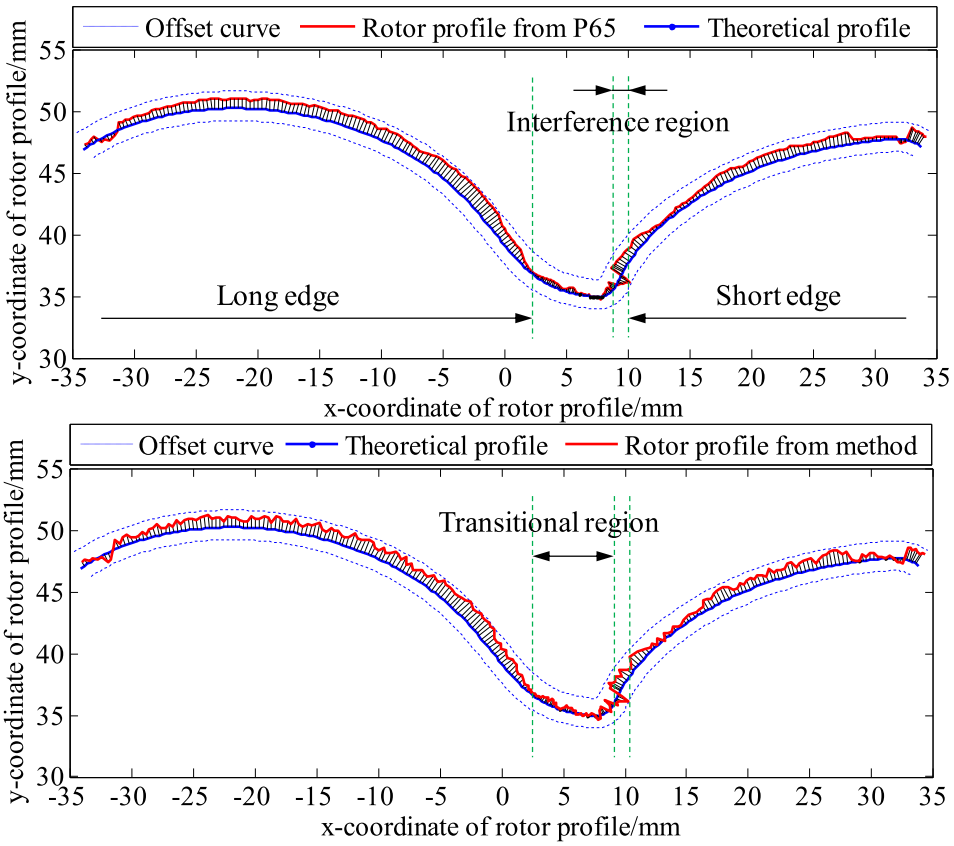

Fig. 19. Comparison and analysis of measurements between LDS and P65.

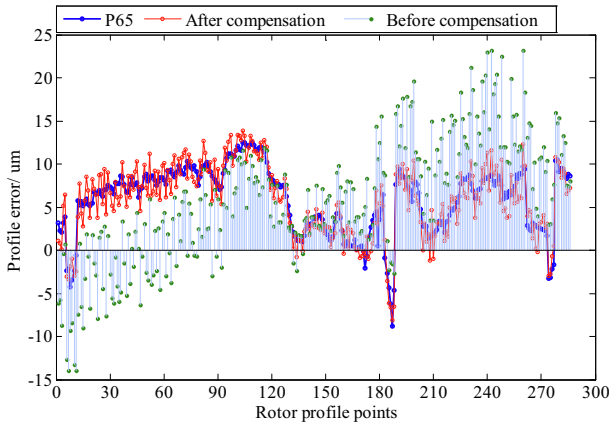

Fig. 20. Comparison of rotor profile errors.

The main reason is that the measurement accuracy of these two parts is greatly affected by the inclination angle, as shown in Fig. 17 and Fig. 8 (b), which has a significant effect on the measurement accuracy. The compensation amount of the transitional curve zone is relatively small; the main reason is that the inclination angle of this part is relatively small, which has little impact on the measurement accuracy.

(3) According to the compensation results caused by deflection angle in the measurement blind area, the compensation effect of the blind zone is better than that of other measurement zones, which demonstrates the feasibility of transforming deflection angle into inclination angle and rotation angle.

(4) Because the measurement results come from the measurement value of the LDS which is stable at the scanning distance h of about 0.5 mm. Therefore, the experimental scheme considers the influence of inclination and deflection angle as well as the error compensation of scanning distance. The accuracy of the error prediction model is further verified.

More detail analyses indicate that the proposed method has better applicability under the same accuracy with contact detection of P65. The specific reasons are as follows: 1) the contact force between the contact probe and the measured workpiece would cause local deformation and affect measuring accuracy. It is necessary to calibrate the probe radius frequently for its accuracy. 2) As an induction element, the contact probe needs radius compensation to reflect the real complex profile, which may lead to correction error. 3) If the curvature radius of the measured point is less than that of the contact probe, the problem of measuring blind angle will arise. 4) To achieve high precision measurement of contact detection, the contact probe has a high price and cannot measure the soft and defective surface. 5) Non-contact measurement is obviously more suitable for online detection of screw rotor.

7. Conclusion

This study analyzed the measurement error caused by the spatial posture of the LDS in the process of non-contact detection of the screw rotor. A laser triangulation measuring method for the screw rotor profile under multi-factor constraints was developed. The proposed method involves 1) the establishment of 4D error compensation model. By analyzing the influence of rotation angle and reflection angle, the model was improved and more principles for LDS installation was formulated. 2) the laser-measurement

trajectory planning for the rotor profile. Aiming at the problem that the complex rotor profile through mechanical and optical path interference causes undesirable blind zones in detection, the detection is conducted along or near the normal direction of each measured point on the rotor profile without any interference to ensure the minimum measurement error. The proposed system and method not only exhibit good performance with acceptable accuracy and reliability for the measurement of screw rotor profile, but also overcome the shortcomings of the traditional contact detection for accuracy loss caused by probe wear and measuring blind angle. We demonstrated a high-precision, effective, and economical method to measure the screw rotor profile, which can be widely used in the online measurement of the screw rotor profile to achieve optimal control of the screw rotor process. To improve the precision of the proposed method:

1) The experimental results show that the characteristics of the measured surface still have a certain impact on the laser measurement accuracy, such as the external temperature and light field, etc., which have not been analyzed in this paper. The error compensation model in this paper can meet the current accuracy measurement requirements of the screw rotor, but if there is a need for higher accuracy, the above factors need to be further studied.
2) In this paper, a laser-measurement trajectory planning for the screw rotor profile was proposed. The experimental results show that it can meet the current accuracy requirements. However, if higher accuracy is needed, there are other measurement methods to be studied besides the proposed method.

Funding statement

This work was funded by National Natural Science Foundation of China (No: 51905459), Project of China Postdoctoral Science Foundation (No: 2019M652256) and Intelligent Manufacturing Integrated Standardization and New Model Application Projects of the MIIT (No. 265 [2018]).

Declaration of Competing Interest

The authors declare that they have no known competing financial interests or personal relationships that could have appeared to influence the work reported in this paper.

References

[1] D. Yan, Q. Tang, A. Kovacevic, et al., Rotor profile design and numerical analysis of 2–3 type multiphase twin-screw pumps [J], Proc. Inst. Mech. Eng. Part E J. Proc. Mech. Eng. 232 (2) (2017) 186–202, https://doi.org/10.1177/0954408917691798.
[2] Y.Q. Zhao, S.D. Zhao, W.F. Wei, et al., Precision grinding of screw rotors using CNC method [J], Inter. J. Adv. Manuf. Technol. 89 (9–12) (2017) 2967–2979.
[3] X.G. Ji, Y. Yang, J. Xue, et al., A RE-based double measurement method for unknown rotor profile of screw compressor [J], Adv. Mech. Eng. 6 (2014), https://doi.org/10.1155/2014/715710 715710.
[4] W.B. Teng, Research on measurement and error evaluation of screw compressor rotors [D], Xiamen University, China, 2016.
[5] Q.C. Zhao, T.L. Yang, X.Y. Yin, et al. Study on measuring parameter lead of screw rotor based on CMM[M], 2013.
[6] Q.B. Tong, C.Q. Jiao, H. Huang, et al., An automatic measuring method and system using laser triangulation scanning for the parameters of a screw thread [J], Meas. Sci. Technol. 25 (3) (2014), https://doi.org/10.1088/0957-0233/25/3/035202 035202.
[7] T. Li, Y. Tan, Z. Zhou, Turbine rotor dynamic balance vibration measurement based on the non-contact optical fiber grating sensing [J], IEICE Electron. Express 12 (12) (2015) 20150380, https://doi.org/10.1117/12.2197785.
[8] L. Zhao, H. Feng, Q. Rong, A novel non-contact measuring system for the thread profile of a ball screw [J], Mech. Sci. 9 (1) (2018) 15–24, https://doi.org/10.5194/ms-9-15-2018.
[9] J. Chao, L. Zhang, Parameters of small pitch thread measured by an intelligent detection method [J], J. Comput. Methods Sci. Eng. 16 (2) (2016) 207–218, https://doi.org/10.3233/JCM-160611.
[10] Z.R. Qiu, Z.K. Su, C.L. Wang, A novel method for measuring the virtual pitch diameter of a thread [J], Measur. Sci. Technol. 29 (11) (2018), https://doi.org/10.1088/1361-6501/aadece.
[11] Z.X. Dong, X.W. Sun, C.Z. Chen, An on-machine precision measurement method for API threads [J], Measur. Sci. Technol. 30 (8) (2019), https://doi.org/10.1088/1361-6501/ab12ac.
[12] M.L. Chen, Compensation of thread profile distortion in image measuring screw thread [J], Measurement 129 (2018) 582–588, https://doi.org/10.1016/j.measurement.2018.07.041.
[13] Z.X. Dong, X.W. Sun, W.J. Liu, et al., Measurement of free-form curved surfaces using laser triangulation [J], Sensors 18 (10) (2018), https://doi.org/10.3390/s18103527.
[14] N. Vukašinović, J. Možina, J. Duhovnik, Correlation between incident angle, measurement distance, object colour and the number of acquired points at CNC laser scanning, Strojniški vestnik J. Mech. Eng. 58 (1) (2012) 23–28, https://doi.org/10.1007/s00170-009-2493-x.
[15] S.S. Li, X.T. Jia, M.W. Chen, et al., Error analysis and correction for color in laser triangulation measurement [J], Optik 168 (2018) 165–173, https://doi.org/10.1016/j.ijleo.2018.04.057.
[16] S.Q. Wu, B. Shen, J.H. Wang, et al., Super-resolution algorithm for laser triangulation measurement [J], Lasers Eng. 38 (3–6) (2017) 385–395.
[17] B. Li, F. Li, H. Liu, et al., A measurement strategy and an error-compensation model for the on-machine laser measurement of large-scale free-form surfaces [J], Meas. Sci. Technol. 25 (1) (2014), https://doi.org/10.1088/0957-0233/25/1/015204 015204.
[18] G.A. Idrobo-Pizo, J.M. Motta, R.C. Sampaio, A calibration method for a laser triangulation scanner mounted on a robot arm for surface mapping [J], Sensors 19 (8) (2019), https://doi.org/10.3390/s19081783.
[19] H.W. Yang, W. Tao, Z.Q. Zhang, et al., Reduction of the influence of laser beam directional dithering in a laser triangulation displacement probe [J], Sensors 17 (5) (2017) 1126, https://doi.org/10.3390/s17051126.
[20] M. Christian, P. Robin, B. Eugen, Accurate light source position estimation for a laser triangulation measurement device using particle swarm optimization [J], Measurement 125 (2018) 406–414, https://doi.org/10.1016/j.measurement.2018.04.087.
[21] C. Lin, X.J. Cao, Y. Fan, et al., Pitch deviation measurement and analysis of curve-face gear pair [J], Measurement 81 (2016) 95–101, https://doi.org/10.1016/j.measurement.2015.12.006.